Carbon Resources Conversion 7 (2024) 100230

Contents lists available at ScienceDirect

Carbon Resources Conversion

journal homepage: www.keaipublishing.com/en/journals/carbon-resources-conversion

Original Article

A novel and sustainable rubber composite prepared from electric arc furnace slag as carbon black replacement

Anna Gobetti [a,*], Giovanna Cornacchia [b], Silvia Agnelli [a], Mattia Ramini [c], Giorgio Ramorino [a]

[a] Materials Science and Technology at Department of Mechanical and Industrial Engineering, University of Brescia, Via 9 Branze 38, 25123 Brescia, Italy
[b] Metallurgy at Department of Mechanical and Industrial Engineering, University of Brescia, Via 9 Branze 38, 25123 Brescia, Italy
[c] Italian Gasket S.P.A., Via Tengattini N.9, (Bs), Paratico 25030, Italy

ARTICLE INFO

Keywords:
EAF slag as non-conventional filler
Carbon black replacement
Rubber composite
Mechanical characterization
Rubber-filler interaction
Industrial waste reuse

ABSTRACT

Carbon black (CB) is the most widely used reinforcing filler for rubber. Nowadays there are several concerns regarding this traditional petroleum-based filler: on one side its environmental footprint is enormous and its production process is no more sustainable and on the other side its price increases annually. For these reasons, sustainable alternative fillers are being studied. In the present research the main waste of the steel industry, namely the steel slag from electric arc furnace (EAF), is investigated as non-conventional filler for a nitrile butadiene rubber matrix (NBR). The slag has been characterized to ensure its safe reuse as filler according to the heavy metals leaching. The slag filled compounds have been characterized and compared to CB filled compounds, in terms of processability by rheometric parameters, mechanical properties, Payne effect, and physicochemical properties to investigate the filler-matrix interaction. From the obtained results, it was shown that EAF slag-filled NBRs are comparable to CB filled NBRs in terms of crosslink kinetics and, when compared at the same hardness level, are comparable in terms of viscosity, stiffness, and elongation at break, while when compared at the same filler volume fraction are similar in terms of compression set and stress relaxation.

1. Introduction

Rubber is a polymer-based material characterized by high elongation and nearly complete recovery of deformation. It is nearly irreplaceable in many applications such as tires, seals, conveyor belts, dumpers, and hoses, just to mention the main important ones. However, in most practical applications, it is essential to use a filler to improve the mechanical properties of these polymeric matrices. CB is the most widely used reinforcing filler for rubber as it can increase more than tenfold the strength of an amorphous elastomer [1].

The first studies of the reinforcement mechanism of CB can be dated back to the 1960s. However, the knowledge of its mechanism still remains fragmentary today [2]. While normally the addition of particle fillers in polymeric matrices increases the elastic modulus but reduces elongation, in elastomeric matrices the addition of CB increases both modulus and elongation at break. The main reasons for this exceptional effect are the very low particle size of CB (<1 μm and with surface area >100 m^2/g), the irregular shape of filler aggregates (filler structure), and the functional groups on the surface (surface activity), which interact with the polymer matrix creating a layer named bound rubber of (partially) immobilized polymer chains on the filler surface [1]. With the presence of CB, the physical properties of rubber compounds, such as tear and tensile strength and elastic modulus, can be improved. CB increases the hardness and viscosity of rubber-based compounds and it is considered the most efficient additive among all filler materials [3]. CB is made up of over 90 % pure form of elemental carbon, which is made up of tiny, mostly spherical carbon particles that fuse together into groups called aggregates. Several aggregates then form clusters that break down during the mixing period of the rubber. Normally, the diameter of the CB particle ranges from 10 nm to 500 nm [2].

Since CB production is based on the partial combustion of heavy hydrocarbons such as coal tar derivate, its carbon footprint is enormous [2]. It has been estimated that the production of 1 ton of CB implies the emission of 2.4 tons of carbon dioxide, compared to 0.8 tons of carbon dioxide per ton of cement during production [4]. Moreover, given the increased demand for rubber quality and the rising price of raw rubber and other component ingredients, the rubber industry has made great efforts to limit costs and increase competitiveness. There are several

* Corresponding author.
E-mail addresses: anna.gobetti@unibs.it (A. Gobetti), giovanna.cornacchia@unibs.it (G. Cornacchia), silvia.agnelli@unibs.it (S. Agnelli), mattia.ramini@italiangasket.com (M. Ramini), giorgio.ramorino@unibs.it (G. Ramorino).

https://doi.org/10.1016/j.crcon.2024.100230
Received 20 September 2023; Received in revised form 1 February 2024; Accepted 7 February 2024
Available online 16 February 2024

concerns regarding the traditional petroleum-based CB filler. On the one hand, the price of hydrocarbons sees a gradual increase every year, and it is subject to fluctuations related to the socio-economical context. The cost of the raw material represents 30–35 % of the total selling price of CB. On the other hand, due to the non-degradability of petroleum-based CB filler, it can cause serious environmental problems. The conservation of the environment and the promotion of recycling [5–7] is a permanent issue, much research is undertaken to reduce the dependence of the CB raw material on fossil fuels and transform it into a sustainable material base. For these reasons, sustainable alternative CB sources such as the pyrolysis of waste tires [8,9] are being studied, as well as reinforcing fillers alternative to CB, such as rice husk ash, peanut shell powder, waste wood, etc. [10–14].

In this study, an industrial waste such as the black electric arc furnace (EAF) slag is proposed as a sustainable filler for the NBR matrix, and its mechanical reinforcing potentialities are compared to those of the most used reinforcing filler, CB. Steel slag features vary according to the type of steel being produced (EAF-C slag from carbon steel production and EAF-S slag from stainless/high-alloy steel production) and its chemical composition may present differences related to the type of scrap used and to the process parameters. In general, the slag can still be assimilated to natural effusive rocks of volcanic origin and consists mainly of a ternary mixture of calcium oxide (CaO), silicon dioxide (SiO_2) and iron oxides (FeO), to which are added, in smaller percentages, other components [15]. The exploitation of steel slag originates from its assimilation to natural hard rocks and therefore from the possibility of replacing inert material in construction sector [16–19]. Although a large part of the black slag is used in the building sector (in 2019 in Europe about 15 % [20]), the reuse of this material as a substitute for a conventional polluting filler for rubber implies a double environmental and economic advantage: on one hand the use of EAF slag as filler reduces the waste landfill disposal promoting a circular economy, and on the other hand it reduces the use of CB, whose production process is not only energy-consuming contributing to global CO_2 emissions significantly, but also utilizes non-renewable feedstock, making it unsustainable [2]. The main issue related to the EAF slag reuse is the leaching of heavy metals, but it was found in previous studies that the incorporation of slag particles into polymeric matrix prevents them from leaching [21–25].

The study aims to compare the effects on the mechanical properties of slag as a total or partial substitute of CB in a rubber matrix. The properties of three standard NBRs (CB filled) have been compared with an NBR filled with only EAF slag (total substitution of CB) and with an NBR filled with equal volume amounts of both EAF slag and CB (partial substitution of CB). EAF slag has been characterized in terms of morphology, chemical composition and particles size distribution. Leaching tests have been performed to check the possibility of a safe reuse of the slag. The comparison between the compounds has been carried out in terms of processability (rheometric parameters), mechanical properties (by hardness test, tensile test, compression test, stress relaxation, permanent compression set and dynamic mechanical analysis), swelling behavior and ageing behaviour. The filler-rubber interaction has been investigated by the measurement of bound rubber, and of non-linear dynamic behavior.

2. Materials and methods

2.1. Materials

Rubber compounds were kindly provided by the industrial compounder Ligom Spa (Grumello del Monte, BG, Italy). All the compounds are based on Nitrile Butadiene Rubber (NBR), are sulfur cured, and reinforced with either CB, EAF slag, or both. Table 1 provides the the compounds' formulation.

CB is a semi-reinforcing furnace carbon black, N772 type, with a density of 1.8 g/cm^3 (reported in the literature [26]) and with a primary particle diameter between 61 and 100 nm, according to ASTM classification.

The slag used as filler is derived from carbon steel production and it is provided by ASONEXT SPA (Ospitaletto BS, Italy) steelmaking plant. The slag has been ground sieved in a grain size <100 μm (3 orders of magnitude larger than CB particle size) and has an average density of 4.1 ± 0.2 g/cm^3 (twice as that of CB) measured on 5 massive slag samples according to the Archimedes principle.

Three main compounds were prepared, all with the same total volume fraction of filler: one with only CB, labeled NBR60 (0 % slag), one where the conventional CB filler has been fully replaced by the same volume of EAF slag as non-conventional filler, labeled NBR45 (100 % slag), and the third one where half of the CB has been replaced by EAF slag, labeled NBR50 (50 % slag) as reported in Table 2. The compounds were prepared using an equal volume fraction of filler, as micromechanical models within the framework of continuum micromechanics suggest that the reinforcement of the composite arises from substituting a portion of the soft matrix with stiffer particles [27]. Consequently,

Table 1
NBR compounds formulation.

Components [phr]	NBR45 (100 % Slag)	NBR50 (50 % Slag)	NBR60 (0 % Slag)	NBR50 (0 % Slag)	NBR45 (0 % Slag)
NBR	100	100	100	100	100
ZnO	5.00	5.00	5.00	5.00	5.00
Stearic acid	0.50	0.50	0.50	0.50	0.50
Antioxidants	2.00	2.00	2.00	2.00	2.00
Plasticizers	16.30	16.30	16.30	16.30	16.30
Sulphur	0.40	0.40	0.40	0.40	0.40
Filler	132	96	60	38	32

Table 2
NBR composites filler type and content, density and hardness.

Materials	Filler [%v/v]		Filler [%wt]		Density	Hardness
	CB	EAF slag	CB	EAF slag	[g/cm^3]	[ShA]
NBR45 (100 % slag)	–	21.0 %	–	50.2 %	1.63	45
NBR50 (50 %slag)	10.5 %	10.5 %	13.5 %	29.0 %	1.43	50
NBR60 (0 % slag)	21.0 %	–	31.9 %	–	1.20	60
NBR50 (0 % slag)	16.0 %	–	23.1 %	–	1.15	50
NBR45 (0 % slag)	14.0 %	–	20.4 %	–	1.14	45

these models predict that the reinforcement will be directly proportional to the filler volume fraction.

Moreover, given the large difference in density between CB and slag (EAF slag density is twice CB density), the formulation with the same weight percentage would introduce further variables. It is important to note that in the labels of compounds, the figure following "NBR" refers to the nominal hardness of the vulcanized rubber in Shore A points, as rubber compounds are usually classified based on their Shore A hardness with a tolerance of ±5 points mostly used in the rubber industry.

Additionally, in order to compare the effects of EAF slag with those of CB in compounds at the same hardness level, other two rubbers filled with only CB were prepared with hardness 45 and 50 ShA: NBR45 (0 % slag) and NBR50 (0 % slag), respectively (see Table 2). It should be noted that the standard NBR (0 % slag) with a hardness of 45 and 50 SHA have been formulated to achieve a comparable hardness to slag-filled compounds. Therefore, the content of other ingredients, such as plasticizers, may not be identical to that of the three compounds formulated with the same volume fraction of filler (NBR45 (100 % slag), NBR50 (50 % slag), NBR60 (0 % slag)). Table 2 reports the NBR composites, the filler content in weight and volume percentage, the rubber density measured according to ASTM D297 [28], and the Shore A hardness measured according to the standard ASTM D2240-3 [29].

The compounds were produced by means of a closed mixer rotating at 30 rpm. Firstly, polymers and additives were introduced and mixed for 30 s. Subsequently, the fillers were added, and the material was discharged at a temperature of 135 °C. The mixture underwent cooling cooled in an open mixer, where pre-dispersed accelerators and pre-dispersed sulfur were incorporated. The plates used to obtain and test the vulcanized samples were compression vulcanized at 160 °C for 20 min.

The production process for the compound, featuring the addition of EAF slag as an unconventional filler to a standard formulation, remains unchanged compared to the conventional process. This approach aligns with the goal of providing an environmentally friendly alternative without introducing complexity to industrial processes.

2.2. EAF slag characterization

X-ray fluorescence (XRF) spectroscopy. The chemical composition of the used EAF slag was determined by X-ray fluorescence spectroscopy by the Thermo Scientific PERFORM'X provided by Thermo Fisher Scientific (Waltham, Massachusetts, United States).

SEM-EDXS analysis. The mineralogical phases of the slag have been identified by Scanning Electron Microscopy (SEM) integrated with Energy Dispersive X-ray Spectrometry (EDXS) (SEM Leo Evo 40, Carl Zeiss, Oberkochen, Germany; EDXS microprobe Link Pentafet Oxford mod. 7060; Oxford Instruments, Oxfordshire, U.K.) after metallographic preparation. The metallographic preparation consists in embedding a bulk sample of slag in resin and subsequently polishing it to achieve a microscope-observable surface The chemical analysis was conducted on the various phases (represented by different shades of grey) enabling the identification of distinct mineralogical phases.

The morphology and the chemical composition of EAF slag particles were analyzed by coating the powders with gold and examining them under a scanning electron microscope.

The chemical composition of the filler particles was investigated using SEM-EDXS [30]. This measurement was performed on small areas of some filler particles using back-scattered electron (BSE) mode. In addition, the elemental distribution of Mg, Al, Si, Ca, Cr, Mn, and Fe was measured.

Additionally, SEM analysis was conducted to determine the slag dispersion in the matrix and particle size distribution by observing the cryogenic surface fracture of slag-filled NBRs. Three samples were analyzed for each composite, and at least three images were taken at magnifications of 200x, 1000x, and 2000x. The particle area of the EAF slag used as filler in the characterized composites was measured using ImageJ image processing software to provide a representative granulometric curve. A total of 5071 particles were analysed.

Leaching behavior. The leaching test was conducted both on the free slag in a grain size lower than 100 μm (as in the composites) and in a grain size lower than 4 mm (according to the standard CEN – EN 12457-2 [31]) and on the final composite materials. In particular, the rubber composite material plate was cut to a particle size of less than 4 mm and the slag dust lost from the cutting surface was removed to evaluate only the inertizing effect of the polymer matrix. As for the characterization of free slag, the amount of tested composite was calculated to maintain the 90 g of slag in a ratio of 1:10 with the liquid (H_2O) for an agitation time of 24 h, according to the standard CEN EN 12457-2 [31]. Then the solution was filtered by a 45 μm filter and analyzed by the ICP Optical Emission Spectrometer to measure the concentration in the solution Cr, Mo, and V (3 measurements).

2.3. Compound characterization

2.3.1. Processability

Rheometric curve. The rheometric parameters of uncured compounds were obtained by the rheometric/vulcanization curves, determined by the oscillating disc rheometer (ODR) machine provided by Gibitre Instruments (Bergamo, Italy) (177 °C, 0.5°, 3 min) according to the standard ASTM D5289 [32]. One sample for each compound was tested.

2.3.2. Physicochemical characterization

Swelling test. Swelling tests were performed on cured samples to evaluate the crosslink density. Rectangular samples of about 500 mg were cut and immersed either in toluene or in tetrahydrofuran (THF) in sealed glass tubes for 48 h at room temperature. The sample was then wiped to remove the solvent on its surfaces and quickly weighed to measure the swollen weight (m_s). This step was followed by drying in an oven at 80 °C to remove small molecular weight substances until reaching stable dried weight (m_d).

The equilibrium swelling index is determined by crosslink density and the attractive forces between solvent and polymer. The theoretical extent of swelling is predicted by the Flory–Rehner equation [33–35] (Eq. (1)).

$$\nu = -\frac{ln\left(1-v_{Rf}\right)+v_{Rf}+\chi v_{Rf}^{2}}{V_s\left(v_{Rf}^{\frac{1}{3}}-\frac{2v_{Rf}}{f}\right)} \quad (1)$$

where:

ν is the crosslink density in mol/cm^3;

V_s is the solvent molar volume (106.52 m^3/mol for toluene and 81.11 m^3/mol for THF);

$f = 4$ for tetra functional network junctions;

χ is the Flory–Huggins solvent–polymer interaction parameter (0.362 for toluene and 0.346 for THF) determined by the Bristow and Watson semi-empirical equation [36–38];

v_{Rf} is the volume fraction of elastomer in the swollen mass, determined according to Ellis and Welding equation [39,40] reported in Equation (2).

$$v_{Rf} = \frac{\frac{m_d-m_f}{\varrho_R}}{\frac{m_d-m_f}{\varrho_R}+\frac{m_s-m_d}{\varrho_S}} \quad (2)$$

where:

m_f is the weight of the filler provided in the material recipe;

m_s is the swollen sample;

ϱ_R is the polymer density (equal to 1.04 g/cm^3);

ϱ_s is the solvent density (toluene 0.866 g/cm^3 and THF 0.889 g/cm^3).

Three samples were tested for each material; the crosslink density is calculated by Eq. (1).

Bound rubber content. The bound rubber content of the unvulcanized compounds was determined after extraction of the unbound materials,

such as the compounding ingredients and free rubber, by soaking compound samples of about 0.3 g in toluene for 7 days (the solvent was renovated after 4 days) at room temperature, followed by drying under suction for 24 h at 40 °C.

The uncured samples of about 250 mg were wrapped in filter paper of known weight. The samples were weighed before immersion and after drying. Known the filler and rubber fraction (determined by thermogravimetric analyses) the bound rubber content (BRC %) was determined according to Eq. (3) [41]:

$$BRC[\%] = \frac{m_d - m_0\left(\frac{m_f}{m_f+m_r}\right)}{m_0\left(\frac{m_r}{m_f+m_r}\right)} \quad (3)$$

where m_0 is the initial sample mass, m_d is the mass of the dry sample after extraction, m_f is the mass of the filler and m_r is the mass of the rubber provided in the materials recipes.

2.3.3. Mechanical characterization

Tensile test. Mechanical tensile tests were performed by an Instron (Pianezza, TO, Italy) test machine (mod. 3366) at room temperature and a cross-head rate of 100 mm/min according to the standard ISO 37:2017 type 2 [42]. The measurement was performed three times for each compound. Elastic modulus was determined as the slope of the stress–-strain curve at a small strain (0–5 % strain).

Ageing behavior. The compounds' ageing behavior was evaluated through tensile testing after 18 months of natural ageing and additional accelerated ageing at 100 °C for 48 h. The method for deriving the percentage change in properties P[%] is shown in Eq. (4).

$$P[\%] = \frac{P_{aged} - P_0}{P_0} \quad (4)$$

where P_0 is the property measured on fresh rubber compound (not aged) and P_{aged} is the property measured on aged materials (18 months of natural ageing and 18 months of natural ageing followed by accelerated ageing at 100 °C for 48 h).

Compression test. Compression tests were performed by Instron 3366 test machine at room temperature and a crosshead rate of 10 mm/min on cylindrical specimens with a nominal diameter of 12 mm and a height of 6 mm. Three loading and unloading cycles up to 25 % deformation were performed before the compression stress strain curve was recorded, according to the standard ISO 7743 [43]. The test was completed at 45 % engineering strain. Three compression tests were performed for each compound.

Stress relaxation. Stress relaxation was characterized in compression by Instron 3366 test machine at room temperature on cylindrical specimens with a nominal diameter of 12 mm and a height of 6 mm. An indicative value of the level of stress relaxation is obtained in this work as the stress loss [%] after 600 s at 25 % imposed strain.

Permanent set. The permanent set was determined in compression (compression set) according to the standard ISO 815 (type B and test method A). It was determined by imposing a compression deformation of 25 % on cylindrical samples (nominal diameter 12 mm and a height of 6 mm) for 24 h at 100 °C. The measure was repeated three times for each material.

The Mullins effect was evaluated in a cyclic uniaxial tensile configuration using a rectangular specimen with nominal dimension 50 × 5 × 2 mm. The testing was conducted on an Instron dynamometer (mod. 3366).

The material underwent 3 loading and unloading cycles, with a maximum deformation of 25 %, followed by an additional 3 cycles at 50 %, maintaining a fixed strain rate of 80 mm/min (the maximum speed without the inertial effect of the crosshead). At the end of the test, the dissipation of the material strained at 25 % and 50 % was calculated as the percentage change in the area under the stress–strain curve (hysteresis area) between the first and third loading cycles. Dynamic mechanical analysis. Dynamic mechanical analysis was performed by a Dynamic Mechanical Thermal Analyser Q800 by TA Instruments (New Castle, United States) in tensile mode at room temperature and a frequency of 1 Hz by varying the applied strain amplitude between 0.01 % and 100 %, to observe the Payne effect and the low and high amplitude plateau of the storage modulus (E′). This test was performed twice on specimens of nominal dimension 2 × 5 × 30 mm.

3. Results

3.1. EAF slag characterization

Chemical composition by X-ray fluorescence spectroscopy (XRF). From existing literature, it is well- documented that the chemical composition and microstructure of slag are influenced by the cooling system adopted during slagging process and the composition of the smelted ferrous scraps [44–46].

Consequently, the intricate interplay between the chemical composition and mineralogical phases of slag exerts a profound influence on its leaching behavior, thereby governing its environmental impact.

Table 3 shows the chemical composition of the EAF slag used as filler in this experimental study, determined by XRF spectroscopy. The main components of slag are iron oxide (Fe_2O_3) and calcium oxide (CaO), followed by silicon oxide (SiO_2), alumina (Al_2O_3), and chromium oxide (Cr_2O_3) in minor quantity. According to Mombelli et al. [47] the percentage by weight of CaO, SiO_2 Al_2O_3 and MgO affects the leaching of V and Cr. In particular, the higher the CaO and MgO fractions, the lower the V concentration in the leachate. The correlation between Ca and V leaching is related to brownmillerite phase ($Ca_2(Al\ Fe)_2O_5$) which is characterized by hydraulic properties and in contact with water hydrates leading higher V leaching in poor Al_2O_3 slag [47].

In Table 3, the basicity indexes were also calculated and are reported due to the important role of basicity which is correlated to the availability of chromium in slags [48].

In steelmaking practice, there are various methods to calculate the basicity index, among the most commonly used are BI2 and BI4 according different formulas explicated in Table 3. The simplest formula BI2 is expressed as the ratio CaO/SiO_2 and by many authors [49–51] it has been associated to the Cr leaching: when BI2 is above 2, as in this analysis, Cr is present as calcium chromite ($CaO{\cdot}Cr_2O_3$), and the slag is prone to Cr leachability.

However, according to Mombelli et al. [47,52,53] the use of a simple binary basicity index (BI2) could not address the leaching behavior of Cr-spinels when formed in low Al_2O_3-MgO, while the more complete formula BI4 takes into account also other elements frequently present in steelmaking slag, and it is expressed as $(CaO + MgO)/(SiO_2 + Al_2O_3)$.

Generally, the formation of spinels is influenced by the basicity of the slag. An increase in slag basicity leads to an increase in Cr concentration, which promotes the formation of unstable spinels due to the presence of Ca and Si, which are non-spinel-forming elements. It was identified in literature studies [50–52] a BI4 range of 2–3, within which the coexistence of Cr-spinel and Ca-chromate ($CaCrO_4$) is observed.

In the present analysis, the basicity index BI4 is determined to be 2.3. This value suggests that the Cr leachability from the coarse slag, as detected by the leaching test (Fig. 6) can be attributed to the presence of an unstable spinel phase and calcium-ferrite known as brownmillerite, which was identified through SEM-EDS analysis (Fig. 3). Furthermore, the low content of spinel forming species such as MgO and Al_2O_3 can promote V leaching [47].

In relation to the leachability of Cr, it has been observed that it appears to be correlated with the spinel formation which is influenced by the cooling rate more than by the chromium oxide content. Indeed, according to Roberti et al. [54], the cooling rate significantly affects the leaching of Cr, thereby modifying the phases in the slags and their solubility, despite the original Cr_2O_3 content.

SEM-EDXS morphology and chemical composition. The characteristics

Table 3
EAF slag chemical composition determined by XRF spectroscopy and basicity indexes. All amounts are reported in [%wt].

SiO_2	Al_2O_3	Fe_2O_3	MnO	CaO	MgO	P_2O_5	TiO_2	Cr_2O_3	S	Na_2O	K_2O	F
9.4	6.4	33.8	6.9	30.2	5.9	0.5	0.4	6.1	0.1	0.4	0.0	0.1

CaO/Al_2O_3 [–]	Al_2O_3/SiO_2 [–]	BI2 CaO/SiO_2 [–]	BI4 $(CaO + MgO)/(SiO_2 + Al_2O_3)$ [–]
4.8	0.7	3.2	2.3

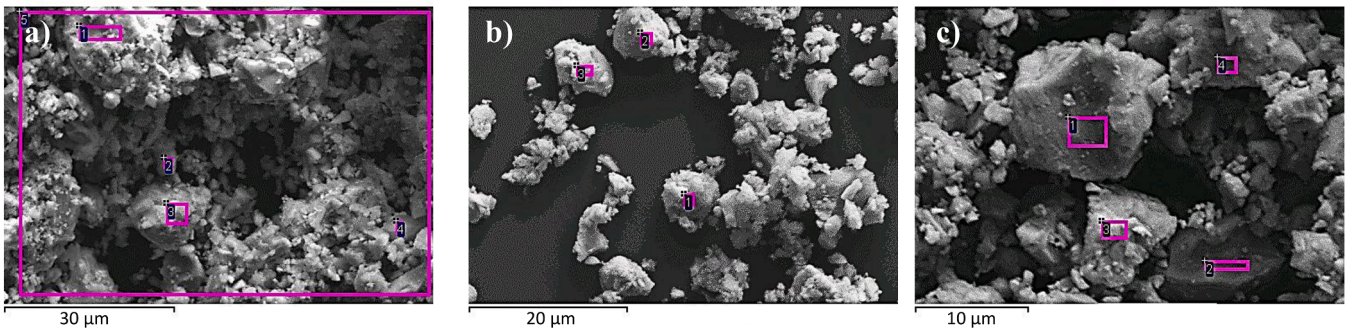

Spectrum	O	Mg	Al	Si	Ca	Cr	Mn	Fe
1	31	7	2		6	2	12	41
2	49		1	12	34	1		3
3	41	3	3	3	18	1	4	27
4	55			5	23			17
5	38	2	3	4	22	4	5	23

Spectrum	O	Mg	Al	Si	Ca	Cr	Mn	Fe
1	36	3	9	7	29	2	4	11
2	29	1	2	10	47	2		10
3	20	3			2	2	6	67

Spectrum	O	Mg	Al	Si	Ca	Cr	Mn	Fe
1	17	4	1		9	3	11	55
2	24	1	1	6	58	2	2	7
3	35	3	4	5	20	2	6	26
4	24	2	2	1	7	3	6	55

Fig. 1. SEM images of EAF slag particles at different enlargements and EDXS analysis. All amounts are reported in wt%.

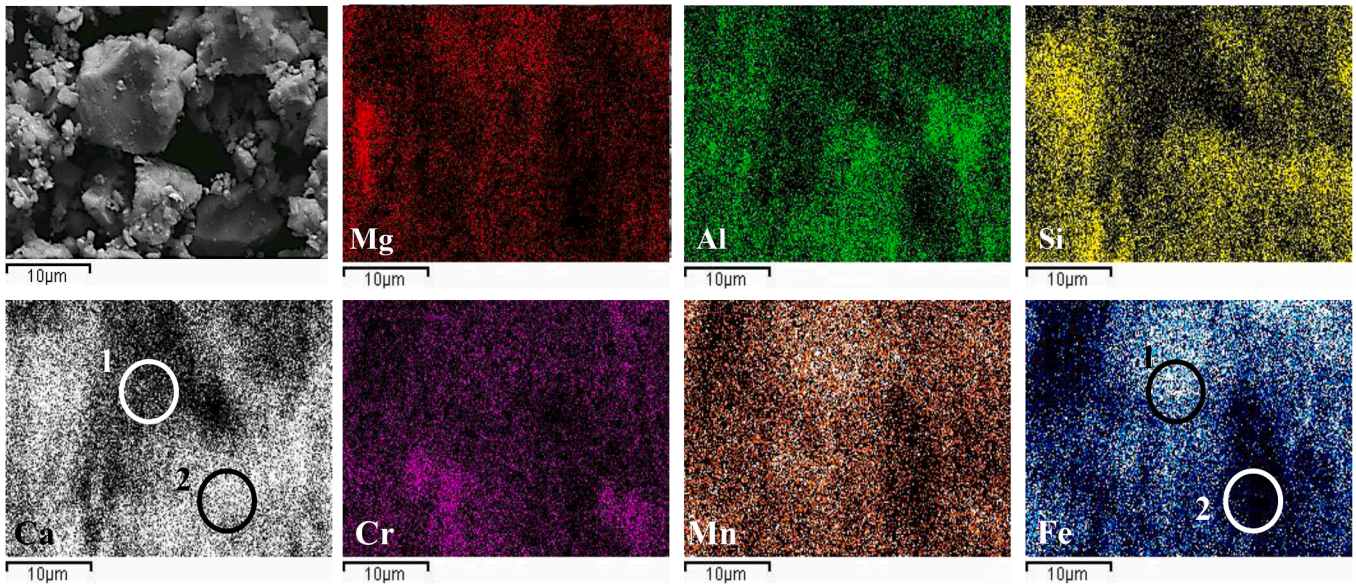

Fig. 2. SEM image of EAF slag particles and map of chemical elements (Mg, Al, Si, Ca, Cr, Mn, Fe) determined through EDXS analysis.

of a filler extend beyond its chemical composition to include its morphology and size. Fig. 1 presents SEM images of EAF slag used as a filler to observe its morphology. The particles exhibit irregular and angular geometry, with smaller particles (in the micron range) tending to deposit onto larger ones. EDXS was used to identify the chemical elements present in small areas of individual particles and aggregates of multiple particles.

The chemical analysis reveals that the predominant chemical elements correspond to those identified through XRF analysis (Table 3). The prominently present elements are Mg, Al, Si, Ca, Cr, Mn, and Fe, accompanied by a substantial oxygen content, indicating the prevalence of oxides, primarily those of Fe and Ca.

To comprehensively identify chemical elements across the entire analysed area, mapping of Mg, Al, Si, Ca, Cr, Mn and Fe was conducted on the same region depicted in Fig. 1c. The results are reported in Fig. 2. It is noteworthy that spectra 1 and 2 (Fig. 1c) are enriched in Ca and Fe respectively, with lower concentration of other elements. This pattern is evident in the elemental mapping of Fig. 2, where the two areas appear to complement each other. The comprehensive elemental mapping facilitates the identification of zones rich in individual elements, thus

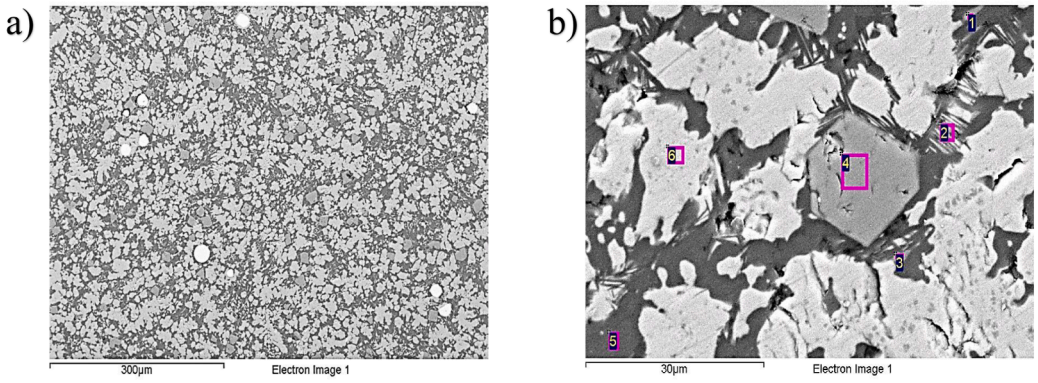

Spectrum	O	Mg	Al	Si	Ca	Ti	V	Cr	Mn	Fe	Phase
1	35,9		7,5	7,2	34,5	6,0		0,7	0,6	7,5	Brownmillerite
2	21,7	3,1	9,9	0,8	7,9			2,2	6,9	47,5	Iron Oxide (MgWüstite)
3	35,5	0,7	14,3	2,6	27,9	5,2	0,6	1,1	1,2	10,9	Brownmillerite
4	24,5	7,6	3,6		0,7			45,9	4,1	13,7	Chromite
5	33,1			16,7	40,7				1,3	8,2	Larnite
6	20,2	4,5	0,8		2,3			3,2	9,8	59,3	Iron Oxide (MgWuestite)

Fig. 3. SEM back-scattered electron (BSE) image of metallographically polished slag sample microstructure at different enlargements. a) EAF slag microstructure at low magnification. b) EAF slag microstructure at high magnification. The table reports EDXS analysis in [%wt] and the corrispective EAF slag microstructure.

validating the EDS spectral analysis towards specific zones.

Mineralogic phases identification by scanning electron microscope (SEM) analysis. The mineralogic phases have been identified by SEM-EDXS analysis. Fig. 3 shows the polished surface of a slag sample at different magnifications with the chemical analysis of the different areas associated to the various phases. In Fig. 3a it is possible to identify some bright steel drops of rounded shape, circumvented by two main phases identified as larnite and magnesio-wüstite and some areas of chromite (in Fig. 3b). At higher magnification, an additional phase has been identified in the form of needle-like structures, which corresponds to the presence of brownmillerite.

Regarding larnite, literature sources [25,54,55] indicate that it undergoes dissolution upon contact with water due to hydration, thereby controlling a significant portion of the Ca concentration in the leachate. This dissolution process, in turn, influences the final pH of the water [53].

Consistent with the findings of Geiβler et al. [38], a correlation between the leaching of Ca and V has been established. Specifically, as the leaching of Ca increases, there is a corresponding decrease in the concentration of V observed in the leachate. As regard chromite, in its stable spinel form, it does not react with water and does not participate in any substantial reactions. Although chromite contains chromium (Cr), it is not directly linked to Cr leaching [54,56].

In accordance with numerous literature studies [53,54,56] brownmillerite is identified as the primary phase associated with Cr leaching. Although its stoichiometric formula does not explicitly include chromium it is possible for chromium to substitute another atom or serve as an interstitial addition, thereby leading to the formation of an unstable phase.

Considering magnesio-wüstite, its dissolution has been found to be influenced by the FeO/MgO ratio [56]. It was observed that no Cr leaching occurred when the FeO content exceeded 70 wt% and no dissolution higher than 60 wt%. According to Mombelli et al. [52] the Cr presence in magnesio-wüstite is unrelated to the Cr leaching. Furthermore, it appears to contribute the reduction of the overall leached Cr.

EAF slag grain size distribution. The size of the filler is a crucial characteristic that significantly influences the performance of the final compound. Fig. 4 illustrates the particle size distribution expressed as both frequency and cumulative distribution based on the surface area of particles measured on the cryogenic fracture surfaces of slag-filled compounds. The analysis revealed that, even though the filler was sieved to a nominal particle size of less than 100 µm, approximately 35 % of the particles have a surface area of around 25 μm^2. Additionally, 95 % of the particles have a surface area less than 625 μm^2. Due to the irregular geometry of the particles, expressing particle size in a linear measurement unit is difficult. Assuming a conservative square geometry, the particles have an average size of less than 30 µm.

SEM micrograph of composites fractur surface. A crucial aspect of the filler in relation to the polymer matrix is its distribution and dispersion within it. Fig. 5 shows the cryogenic fracture surface observed under SEM at different magnifications for NBR60 SHA (0 % slag), NBR50 SHA (50 % slag), and NBR45 SHA (100 % slag). The noticeable difference in dimensions between the carbon black (not visible in Fig. 5a) and the clearly identifiable slag particles present in the NBR 50 (50 % slag) and NBR 50 (100 % slag) compounds (Fig. 5b and c) is immediately apparent. Additionally, the figure shows that the slag particles are well-distributed and dispersed within the polymer matrix. The enhances adhesion of the matrix, is particularly notable as the particle size decreases. This is evident in well-incorporated particles that do not detach, as observed in coarser particles.

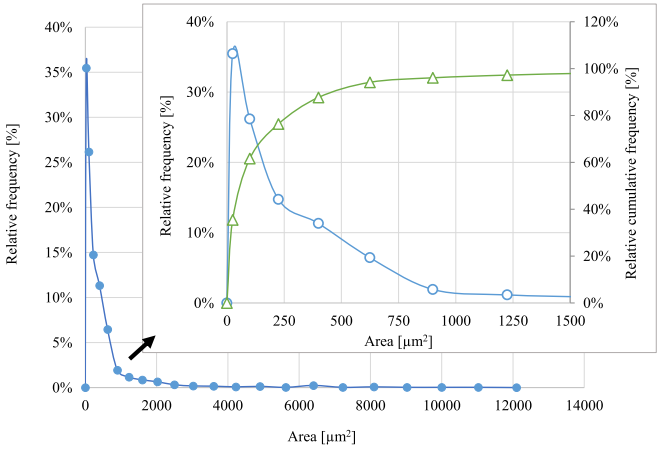

Fig. 4. EAF slag particles size distribution expressed as frequency and cumulative frequency function of slag particles area embedded in the NBR matrix.

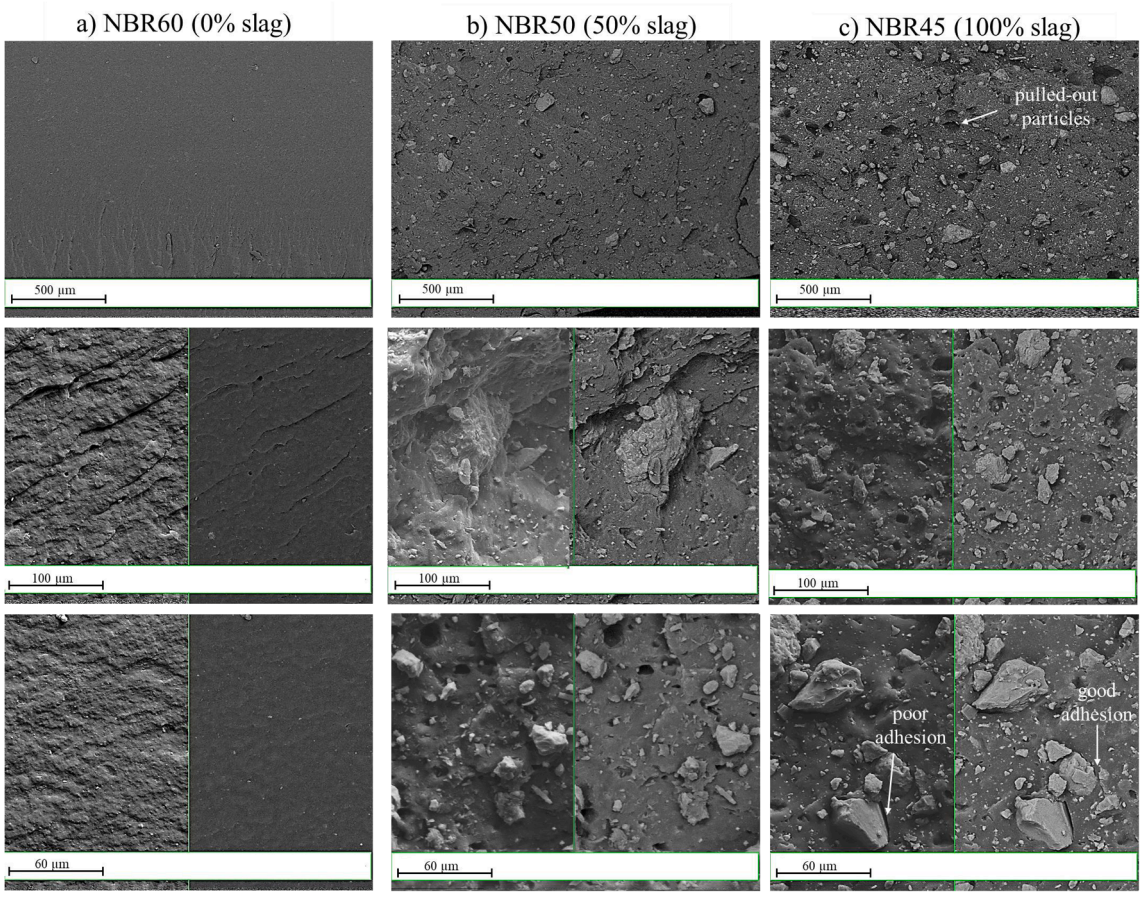

Fig. 5. SEM micrograph (left side of the image) and backscattering (right side of the image) of cross sections of specimens broken in liquid nitrogen. a) Micrograph of NBR60 (0% slag); b) micrograph of NBR50 (50% slag); c) micrograph of NBR45 (100% slag).

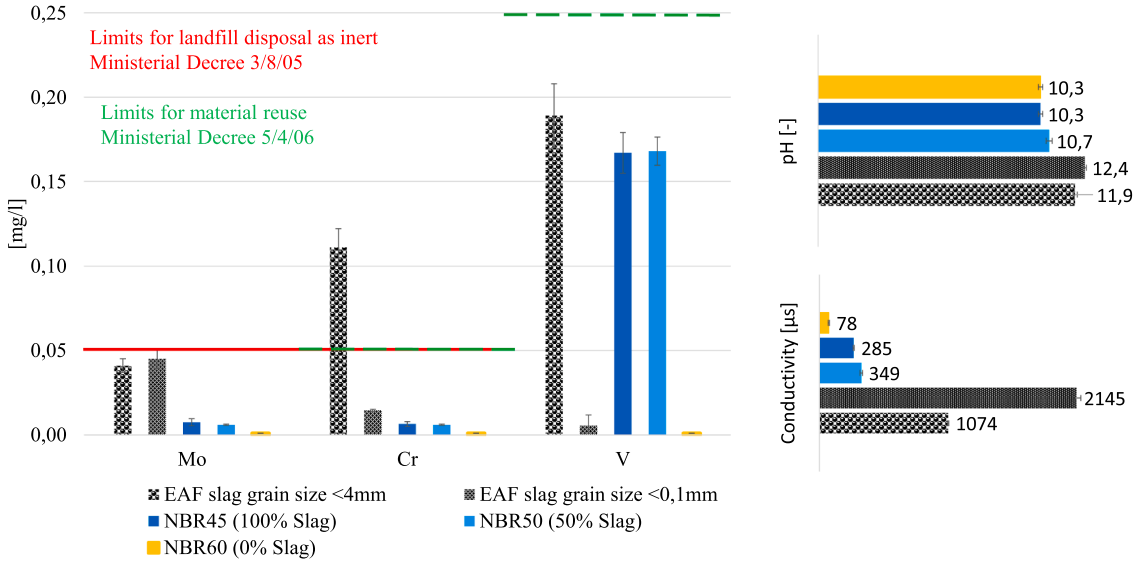

Fig. 6. Leaching test CEN EN 12457–2 results of free EAF slag (grain size < 4 mm), free EAF slag (grain size < 0.1 mm), NBR filled with EAF slag at 30 %v/v (grain size < 0.1 mm), EAF slag block incorporated into NBR and standard NBR.

Leaching test. The leaching behavior of EAF slag, both free and incorporated into the NBR matrix, is shown in Fig. 3. As aforementioned, free slag leaching test has been conducted both according to the standard CEN-EN 12457-2 [31] (slag grain size lower than 4 mm) and on slag grain size lower than 100 µm. Several studies demonstrated a correlation between the slag grain size and its leaching behavior [21,54,57]. In fact, a higher surface/volume ratio of slag particles leads to increased leaching of elements due to a larger contact area between the solid and liquid phases. Nevertheless, while this was observed for Mo leaching, it was found that EAF slag with a coarse grain size leaches

higher amounts of Cr and V compared to fine grained slag (with a grain size lower than 100 μm). This behavior can be related to the influence of basicity as detailed in XRF analysis. A higher dissolution of larnite implies a higher Ca concentration in the leachate and in turn reduces the V leaching [58]; analogously also other elements move into the leachate varying pH and more evidently the electrical conductivity. This is evident as high larnite fraction increases the ion concentration (Al, Ca and Ba) in the leachate; since electrical conductivity is a non-selective ions measurement method, it is highly sensitive to the slag grain size.

Concerning the leaching test results of EAF slag incorporated into NBR it is noticeable that it is well below the threshold limits imposed by the Italian legislation both as for material reuse (Ministerial Decree 5/4/06 [59]) and for disposal as inert material (Ministerial Decree 30/8/05 [60]).

The different V leaching between free fine slag and fine slag incorporated in the polymeric matrix could be attributable to the high heterogeneity of the slag and its sampling, nevertheless the inertizing effect of the polymer matrix is still appreciable.

3.2. Composites characterization

3.2.1. Processability

Rheometric curves and parameters. In order for rubber to show its well-known elastic behavior, raw rubber compounds must be vulcanized, i.e. the molecular chains must be weakly crosslinked. In particular, vulcanization or curing is a technical term used when the crosslinking agent is sulfur. The study of vulcanization kinetics is very important to determine the operating window, the production process parameters setup, and very useful information can be acquired by the parameters collected from the curing rheometric curves.

Fig. 7 shows a comparison of measured rheometric curves (Fig. 7a) and parameters (Fig. 7b) for rubber compounds filled with CB, specifically standard compounds known as NBR60 (0 % slag), NBR50 (0 % slag), NBR45 (0 % slag), as well as NBR compounds filled with EAF slag NBR50 (50 % slag), NBR45 (100 % slag). The rheometric parameters under consideration include the minimum measured torque (M_L) which is roughly related to the rubber compound viscosity, the highest torque (M_H) which relates to the physical properties of the cured material (cured state), and the time related to scorch (t_{s2}) and the curing kinetics (t_{90}). The parameter t_{s2} represents the time required to increase M_L of 2 dN while t_{90} indicates the time needed to achieve the 90 % complete state of cure (from M_L to M_H). These parameters hold significance in assessing industrial operating window. On one hand, the material should vulcanize rapidly to reduce cycle time, increase productivity and lower costs. On the other hand, if vulcanization occurs while the material is still flowing in the channels, it may result in the production of defective parts.

The comparison reported in Fig. 7 allows the following considerations: (i) M_L and M_H of CB filled rubber compounds decrease with decreasing the filler content due to a higher volume fraction of polymer; (ii) M_L of EAF slag filled NBRs is significantly lower than that of NBR 60 (0 % slag) although the equal filler volume fraction, and it is slightly lower than that of CB filled NBRs at equal hardness. This discrepancy can be attributable to the different fillers surface area, to which the polymer can adhere and be adsorbed, leading to a mobility reduction. Regarding the curing kinetics: (iii) both at an equal filler volumetric fraction and at equal hardness (especially hardness 50 ShA), the scorch time (t_{s2}) of slag filled compounds shows a slight extension; (iv) the cure time, associated to t_{90}, remains unaltered.

The findings related to the rheometric curve parameters reveal a good processability of the slag filled compounds thanks to a lower viscosity and extended scorch time without affecting the global production cycle time without manifest reversion in rheometric curves.

3.2.2. Physicochemical characterization

Swelling test. Fig. 8shows the crosslink density of vulcanized CB filled NBRs (0 % slag), and slag filled NBR45 (100 % Slag) and NBR50 (50 % slag) determined by swelling test performed both in toluene and THF.

The investigation revealed that the crosslink density, determined using toluene as the solvent, was slightly higher compared to the crosslink density determined using THF. However, despite this small difference, the results obtained from both solvents were in good agreement, indicating a high level of test reliability.

When comparing compounds with equal filler volume fraction, it was observed that the crosslink density is higher in compounds containing CB (i.e., NBR60 (0 % slag) and NBR50 (50 % slag)) compared to NBR45 (100 % slag). This can be attributed to the well-known CB surface activity [61], as well as the coarser size and unstructured geometry of slag particles. The latter characteristics lead to reduced interaction between the polymer and the filler, resulting in a lower crosslink density and diminished macromolecular mobility. This effect is evident both in terms of hydrodynamic effects and the bound rubber. As expected, in CB filled NBRs with increasing the filler content (from NBR45 (0 % slag) to NBR 60 (0 % slag)) the crosslink density increases due to greater surface

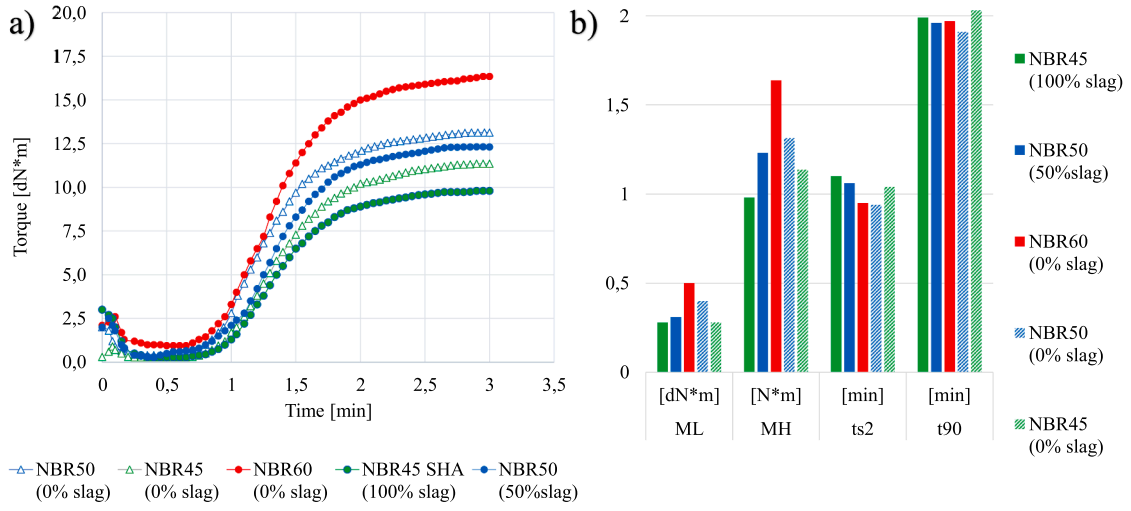

Fig. 7. Rheometric curves and parameters of CB filled NBR60 (60 ShA), NBR50 (50 ShA), NBR45 (45 ShA), 100% EAF slag filled NBR and 50% EAF slag filled NBR. a) Rheometric curves; b) Rheometric parameters: ML and MH are the lowest and highest torque, respectively, measured by the rheometer; ts2 is the time required to increase ML of 2 dN and t90 is the time required to reach the 90% of complete cure.

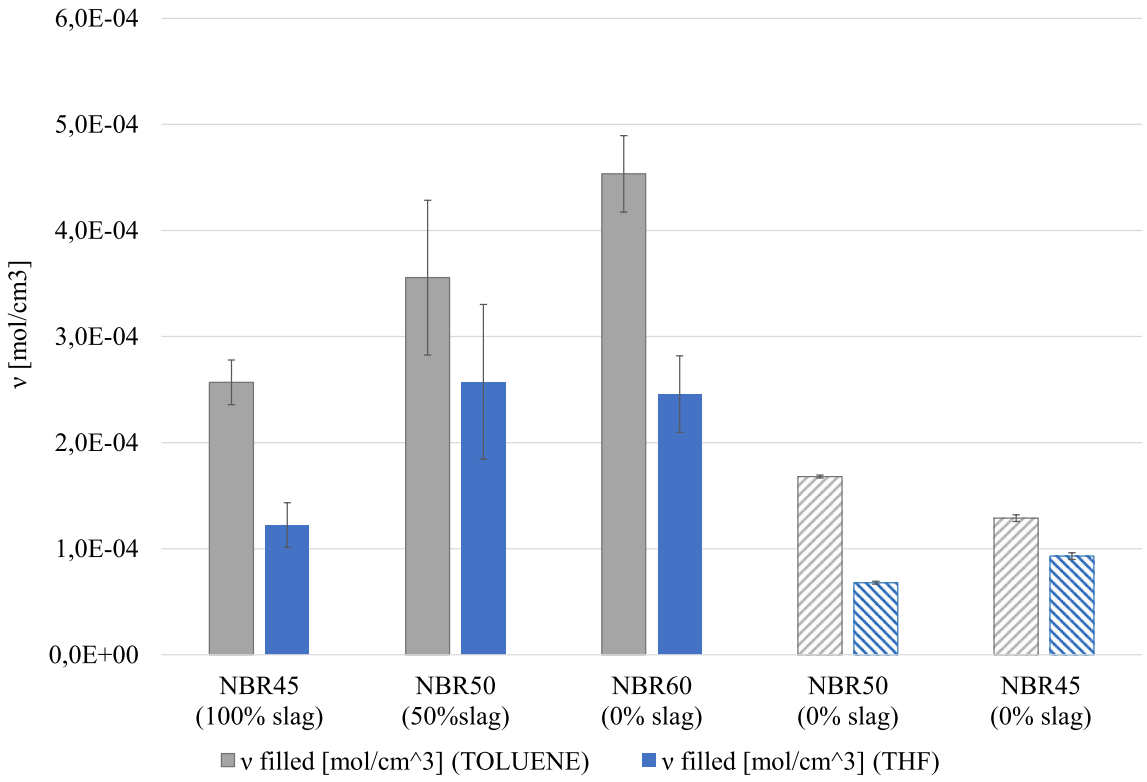

Fig. 8. Crosslink density of CB filled NBR60 (60 ShA), NBR50 (50 ShA), NBR45 (45 ShA), 100 % EAF slag filled NBR and 50 % EAF slag filled NBR. Swelling test 48 h, Toluene and THF at room temperature.

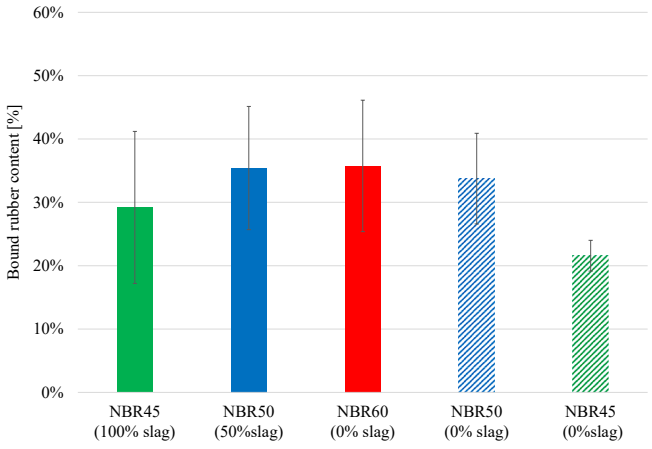

Fig. 9. Bound rubber content of CB filled NBR60 (60 ShA), NBR50 (50 ShA), NBR45 (45 ShA), 100 % EAF slag filled NBR and 50 % EAF slag filled NBR. Immersion in toluene for 7 days.

of interaction promoting the bound rubber formation [62,63]. It is interesting to notice that at equal compounds hardness the slag filled NBRs present a higher crosslink density downstream to lower swelling. As the crosslink density determined by the Flory Rehner equation [64] is based on the experimental results of the swelling behavior, the aforementioned behavior of the materials at equal hardness can be related to a higher swelling of the CB filled elastomers due to the lower filler volume fraction.

Bound rubber content. To investigate deeply the filler-matrix interaction the bound rubber content is determined (Fig. 9). The bound rubber content serves as a measure of the uncured polymer fraction whose macromolecules are constrained to the filler surface and cannot be detached even by a good solvent. The experimental results revealed no significant differences between the different fillers at equal volume fraction. However, it is important to highlight that the slag surface area is significantly lower than that of CB, indicating a potential interaction between the NBR and slag. The EAF slag has an ionic chemical nature due to presence of metal oxides, therefore an ionic interaction with the acrylonitrile monomer of the NBR elastomer can be hypothesized. For example, the hydrophilic surface of silica may create an interaction with acrylonitrile groups in NBR. Regarding the CB filled NBRs, consistently with the swelling test results (Fig. 8), it was observed that a decrease in the CB content, corresponded to a reduction in the surface area of interaction between the filler and the matrix. Consequently, this led to a decrease in the measured bound rubber content.

3.3. Mechanical characterization

Tensile test. Fig. 10 shows the stress strain curves of NBR compounds at equal filler volume fraction, namely NBR60 (0 % slag), NBR45 (100 % slag) and NBR50 (50 % slag) as solid lines. The NBR compounds with hardness equal to that of slag filled NBRs, are represented as dotted lines.

As expected, NBR60 (0 % slag) shows the highest tensile strength, which is proportionally reduced by increasing the slag content. Analogously, it decreases with decreasing the standard NBRs hardness. It is interesting to note that the substitution of CB with slag does not significantly reduce the elongation at break. Conversely, in the case of NBR 50 % Slag, it is slightly increased. As regards the comparison between the slag filled NBRs and the standard ones at equal hardness, NBR50 (50 % slag) exhibits a higher elongation at break (approximately + 25 %) but a lower stress at break (approximately −15 %). NBR45 (100 % slag) exhibits a similar elongation at break, but markedly lower stress at break (approximately −65 %). Nevertheless, it is possible to affirm that NBR50 (50 % slag) shows superior tensile behavior compared to the standard NBR45 (0 % slag).

Fig. 10b shows the tensile elastic moduli of the tested materials: the modulus (E) was determined as the slope of the tangent to the first linear

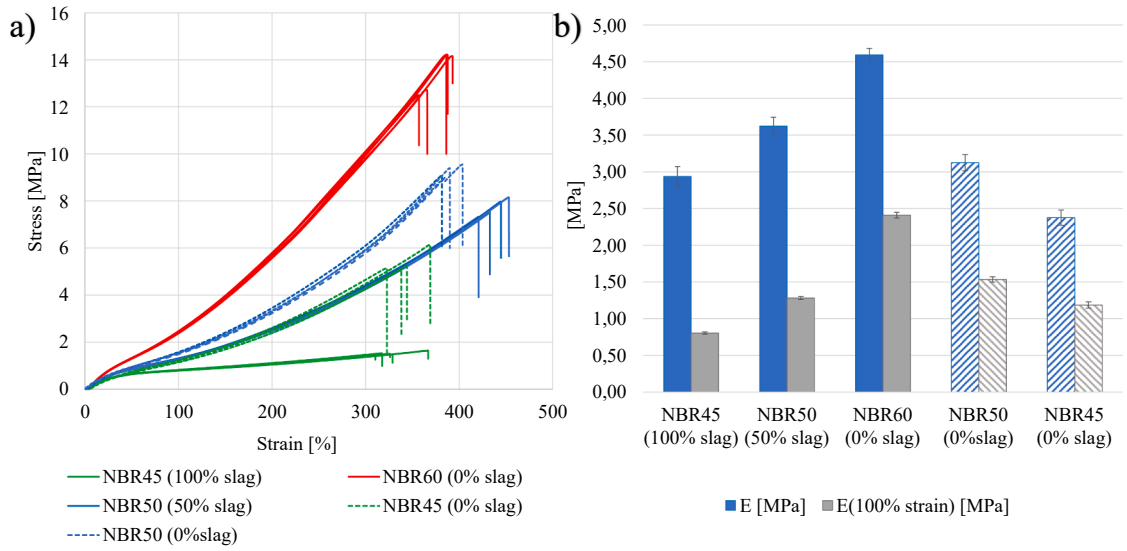

Fig. 10. a) Engineering stress optical strain tensile curves of CB filled NBR (60 ShA), NBR50 (50 ShA), NBR45 (45 ShA), 100 % EAF slag filled NBR and 50 % EAF slag filled NBR. Displacement rate 100 mm/min, room temperature, ISO 37 type 2; b) Initial elastic modulus and secant elastic modulus at 100 % strain of CB filled NBR (60 ShA), NBR50 (50 ShA), NBR45 (45 ShA), 100 % EAF slag filled NBR and 50 % EAF slag filled NBR.

section of the stress strain curve (up to 5 % strain), while E(100 %) was determined as the slope of the secant at 100 % strain. It was observed, as expected, that NBR60 (0 % slag) exhibits the highest moduli. Furthermore, it was found that the EAF slag filled NBR displays a modulus slightly higher than that of the standard NBR at equal hardness level.

However, when considering E(100 %), the modulus of the slag-filled NBRs is slightly lower than that of the standard CB filled NBRs at equal hardness.

Based on the results obtained from the tensile test, it can be concluded that the partial CB replacement with EAF slag does not lead a significant drop in tensile properties when comparing materials of equal hardness. Moreover, it is possible to state that the NBR 50 % slag presents improved tensile properties with respect to standard NBR hardness 45 ShA.

Ageing behaviour. The study evaluated the tensile behavior of compounds containing chemical elements not found in conventional fillers, such as Fe, Mn and Cr. The evaluation was based on the percentage change in tangent modulus, secant modulus at 100 % strain and strain at break after natural ageing in air for 18 months and further accelerated ageing at 100 °C for 48 h. The results are shown in Fig. 11.

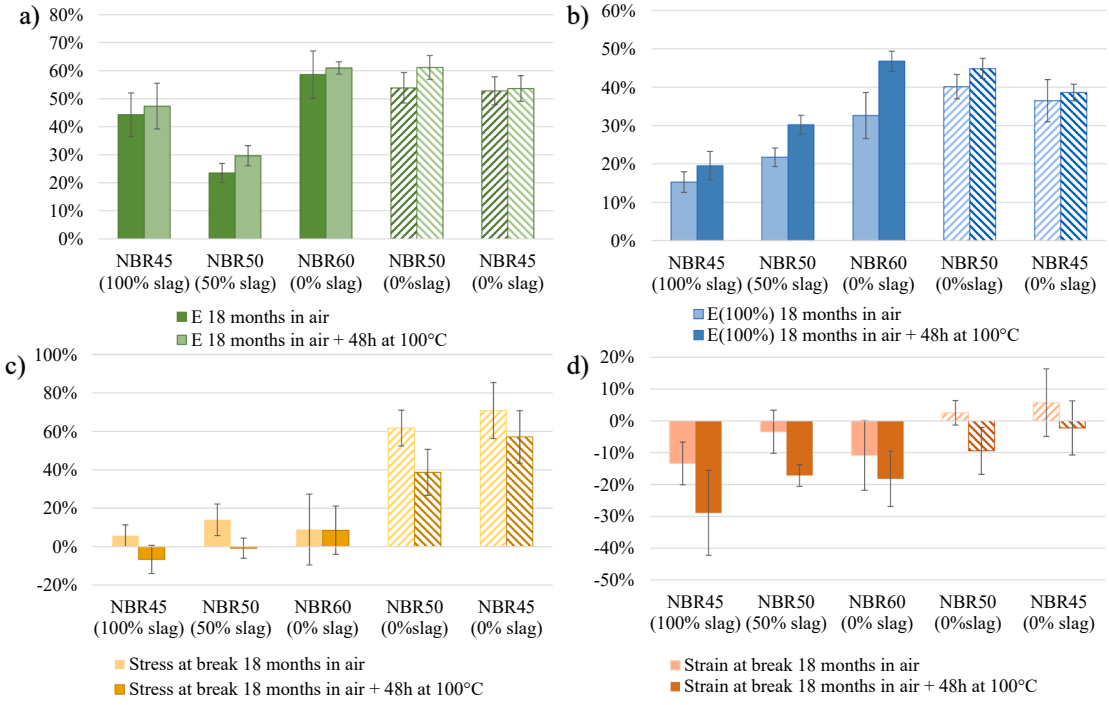

Fig. 11. Percentage change in tensile properties of CB filled NBR (60 ShA), NBR50 (50 ShA), NBR45 (45 ShA), 100 % EAF slag filled NBR and 50 % EAF slag filled NBR after natural ageing in air for 18 months and further ageing at 100 °C for 48 h; a) tensile modulus; b) secant modulus at 100 % strain; c) stress at break; d) strain at break.

In general, it can be seen that the materials stiffen (increase in E and E(100 %)). This behavior is well known and is due to various factors such as oxidative cross-linking, migration of additive particles on the surface and changes in the mechanical properties of the rubber. Thermal oxidative ageing causes heterogeneous oxidation of NBR, resulting in cross-linking and an increase in tensile modulus, while tensile elongation tends to decrease [65]. This trend can be attributed to further cross-linking of the polymer chains, resulting in a tighter and denser molecular network. This limits chain movement and reduces the flexibility and elongation capacity of the NBR without breaking. In addition, any plasticizing additives mixed into the compound can leach out over time. Their loss leaves a stiffer and more fragile rubber network with lower ultimate elongation.

For NBR standards (0 % slag), there is no significant difference in stiffness for different degrees of hardness. However, NBRs containing slightly more plasticizer (NBR50 and NBR45) show a significant increase in stress at break and a slight reduction in elongation at break. This can be attributed to a lower loss of plasticizer with an increase in cross-linking density.

For NBRs filled with slag, the percentage increase in E(100 %) after ageing is inversely proportional to the slag content. Similarly, the tensile modulus (E) of the NBRs filled with slag, especially NBR50 (50 % slag) shows a smaller percentage increase after aging compared to NBR60 (0 % slag). After ageing, the percentage change in stress and strain at break was not significantly different between NBR60 (0 % slag), NBR50 (50 % slag), and NBR45 (100 % slag). The only exception was that NBR45 (100 % slag) showed a slightly greater reduction in strain at break compared to the others.

These results suggest that the chemical elements present in the slag do not significantly accelerate compound ageing. In fact, they may even slow it down, especially in the NBR50 material (50 % slag), where the percentage variation of the observed properties is always lower or at least equal to that of CB filled NBR (0 % slag).

Compression test. Among the main applications of NBR compounds are seals and gaskets, where the main stress state is compression. Therefore, the compressive behavior of these rubber compounds has been investigated through various testing methods, including short term evaluations such as the static compression test, as well as long term assessments such as stress relaxation and permanent set tests.

Fig. 12a illustrates the compression stress strain curves of NBR60 (0 % slag), NBR45 (100 % slag) and NBR50 (50 % slag) represented by solid lines. In order to assess the mechanical behavior of EAF slag filled NBRs in comparison to standard NBRs (0 % slag) and explore the potential for producing more sustainable materials, the compression stress strain curves of standard NBR compounds (NBR45 (0 % slag) and NBR50 (0 % slag)) with hardness 45 ShA and 50 Sha respectively are also reported in Fig. 7a, represented by dotted lines.

The investigation revealed that NBR60 (0 % slag) shows the highest stress strain curve in compression. However, it is interesting to note that NBR45 (100 % slag) exhibits a similar compressive behavior of standard NBR50 (0 % slag) and displays superior compressive performance with respect to standard NBR45 (0 % slag). Fig. 12b shows the compression elastic modulus of the materials under investigation. The compression elastic modulus was determined by calculating the slope of the tangent to the first section of the stress strain curve (up to 3 % strain). The results indicated, as expected, that NBR60 (0 % slag) exhibited the highest compressive modulus. However, it is noteworthy that the EAF slag filled NBR displayed a slightly higher compressive modulus compared to standard NBR at the same hardness level.

Based on the results obtained from the compression test, it is possible to state that the EAF slag filled NBRs present comparable or potentially enhanced compression properties compared to standard NBRs at equivalent hardness. This outcome offers significant economic and environmental advantages.

Stress relaxation. Fig. 13a shows the stress relaxation curves as a function of time at a 25 % strain of CB filled NBRs (0 % slag), and slag filled NBR45 (100 % Slag) and NBR50 (50 % slag). The compression test results revealed that with increasing the compounds hardness the stress reached at 25 % strain increases, according to the compression test results. However, it is interesting to notice that the stress relaxation curves of slag filled NBRs and CB filled NBRs at equal hardness levels are almost perfectly overlapped. Fig. 8b presents the stress relaxation expressed as the percentage of stress reduction at 300 s of the tested materials. It was observed that the stress relaxation of EAF slag filled rubber compounds was comparable to that of standard NBR60 (0 % slag). Moreover, it is slightly higher compared to that of standard NBRs equal hardness levels (NBR45 (0 % slag) and NBR50 (0 % slag)). This behavior can be attributed to the lower rubber fraction present in NBR60 due to higher CB content. At a 25 % strain, the higher hardness of NBR60 (0 % slag) results in localized higher stress on the lower rubber fraction compared to NBR45 (0 % slag) and NBR50 (0 % slag). In the same way, the comparison at equal hardness highlights a lower stress relaxation in

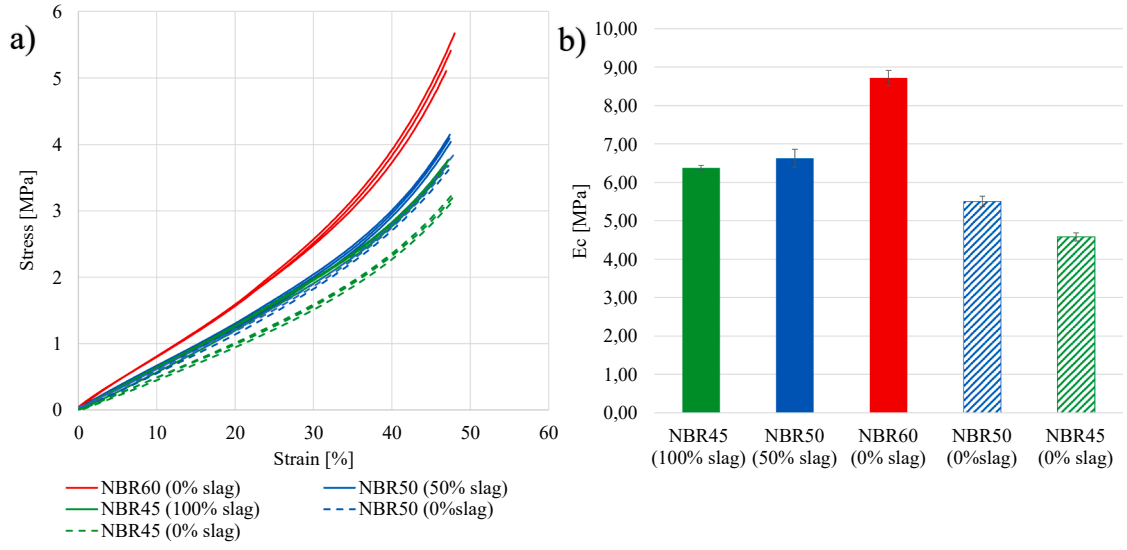

Fig. 12. a) Engineering stress strain compressive curves of CB filled NBR (60 ShA), NBR50 (50 ShA), NBR45 (45 ShA), 100 % EAF slag filled NBR and 50 % EAF slag filled NBR. Displacement rate 10 mm/min; b) Initial elastic modulus of CB filled NBR (60 ShA), NBR50 (50 ShA), NBR45 (45 ShA), 100 % EAF slag filled NBR and 50 % EAF slag filled NBR.

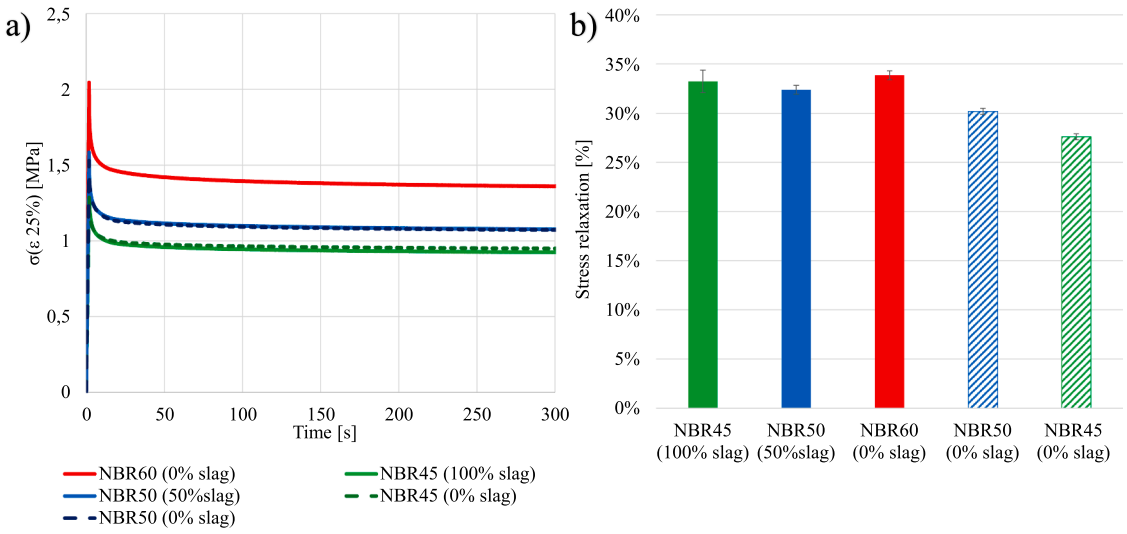

Fig. 13. a) Stress relaxation curves as function of time of CB filled NBR (60 ShA), NBR50 (50 ShA), NBR45 (45 ShA), 100 % EAF slag filled NBR and 50 % EAF slag filled NBR; b) Stress relaxation in percentage of CB filled NBR (60 ShA), NBR50 (50 ShA), NBR45 (45 ShA), 100 % EAF slag filled NBR and 50 % EAF slag filled NBR, after 300 s at 25 % strain.

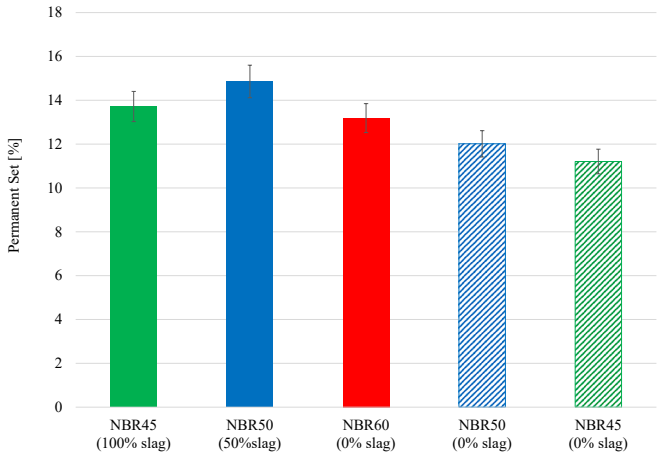

Fig. 14. Compression set of CB filled NBR60 (60 ShA), NBR50 (50 ShA), NBR45 (45 ShA), 100% EAF slag filled NBR and 50% EAF slag filled NBR.

standard NBRs (CB content 14 %v/v and 16 % v/v) due to the lower filler volume fraction with respect to the slag filled NBRs (21 %v/v).

Permanent set. Permanent set is an additional method employed to assess the stress relaxation characteristics of a rubber material. It evaluates the material ability to recover an imposed deformation maintained for a fixed time at a designated temperature.

The permanent set in compression, i.e. the compression set as the permanent deformation of CB filled NBRs (0 % slag), and slag filled NBR45 (100 % Slag) and NBR50 (50 % slag) is illustrated in Fig. 14.

It was observed that, at an equal filler volume fraction, the rubber's ability to recover its original dimensions is only minimally reduced with increasing slag content. This reduction is reflected by an increase in compression set.

As regards the comparison at equal hardness, it is possible to notice that the slag filled NBRs exhibit higher compression set values. Moreover, the results obtained for NBR45 (0 % slag) and NBR50 (0 % slag) appear in agreement with the stress relaxation results. Nevertheless, it is important to highlight that a compression set (at 100 °C, for 24 h, at 25 % strain) lower than 15 % is considered indicative of good elastic behavior.

The experimental results regarding the viscoelastic behavior of the compounds, specifically stress relaxation and permanent set, were found to be mutually consistent. In particular it was observed that at equal filler fraction, despite the notable difference in filler particle size affecting the surface area of interaction with the matrix, no significant differences have been detected. On the contrary, at equal hardness, it was found that the slag-filled compounds are more prone to rearrange their internal material structure when subjected to an enforced deformation.

Mullins effect. Rubber compounds exhibit a viscoelastic effect characterized by stress softening and recovery hysteresis during cyclic deformations. When subjected to cyclic strain-controlled loadings, elastomers reinforced with fillers demonstrate significant softening. While extensively investigated, the underlying mechanism remains unclear [66]. The physical explanation of the Mullins effect involves factors, including bound rupture, molecules slipping on the filler surface (due to weak filler-matrix interaction resulting from low adsorption), filler aggregate rupture, and disentanglements, as well as the double layer model describing the double-layer structure of bound rubber embedded in a crosslinked rubbery matrix, according to the literature [66].

Fig. 15 shows the experimental results of the stress–strain curves under cyclic loading and the percentage variation of the relative hysteresis area between the first and third cycles.

It is observed that compounds with the same volume fraction of filler exhibit a larger hysteresis area at the first cycle than the two standard compounds with the same hardness (NBR50 (0 % slag) and NBR45 (0 % slag)). The results suggest higher material dissipation, likely due to a different interaction between the polymer and filler. This could be attributed to differences in surface area and interaction strength. The coarser particle size of the slag, compared to carbon black, may be responsible for the observed behaviour, possibly due to the sliding of macromolecules on the surface of the slag particles.

From the third loading cycle onwards, the behaviour becomes stable. The percentage variation of the hysteresis area shown in Fig. 15b has been evaluated. It can be observed that, especially at 50 % strain, the NBR compounds at equal filler volume fraction show a dissipation decrease, while in carbon black-filled compounds it decreases slightly as the CB content decreases. It is important to note that the analysis of the hysteresis area at 50 % strain was conducted after a preliminary series of loading cycles at 25 %. As a result, the material has partially settled, resulting in a smaller percentage change.

Dynamic mechanical analysis. The dynamic-mechanical behavior is investigated by analyzing the tensile storage modulus (E') as a function

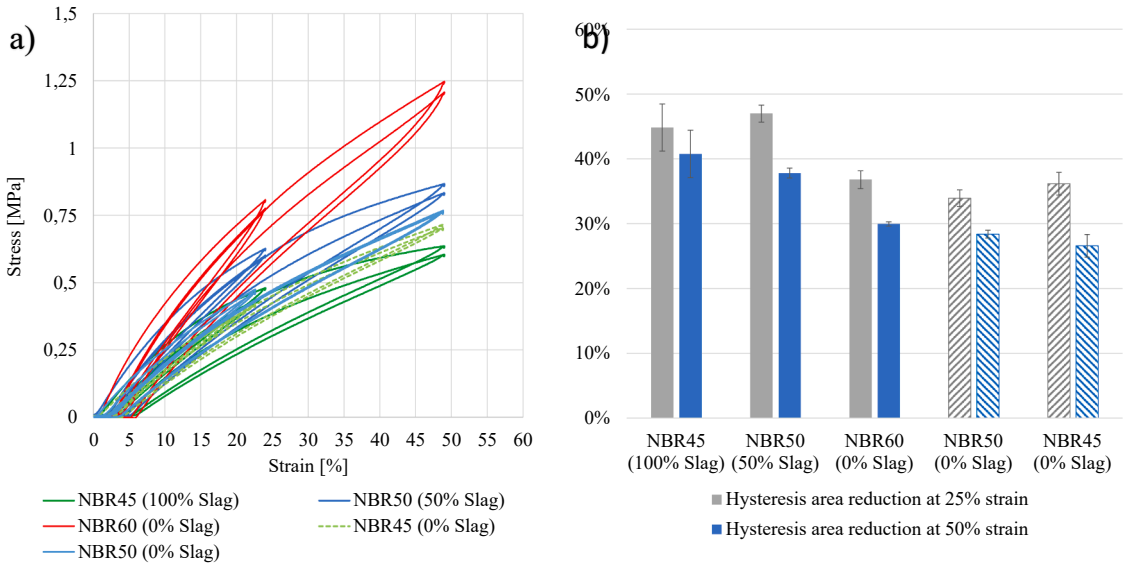

Fig. 15. a) Uniaxial tension stress strain curve during the first and the third cycles of cyclic loading at different strain levels (25% and 50%) of CB filled NBR60 (60 ShA), NBR50 (50 ShA), NBR45 (45 ShA), 100% EAF slag filled NBR and 50% EAF slag filled NBR; b) dissipation at different strain levels (25%, 50%) calculated as the percentage change in the area subtended by the stress–strain curve between the first and third load cycles.

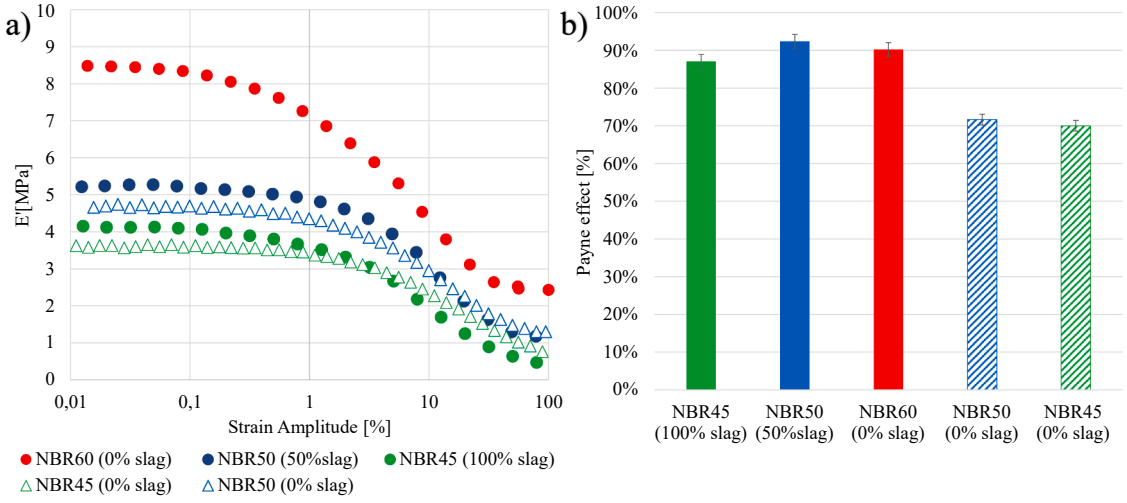

Fig. 16. a) storage modulus (e′) as a function of strain amplitude and b) payne effect [%] as the percentage reduction of the storage modulus from the low deformation amplitude plateau to the high deformation amplitude plateau of CB filled NBR (60 ShA), nbr50 (50 ShA), nbr45 (45 ShA), 100 % EAF slag filled NBR and 50 % EAF slag filled NBR (1 Hz, room temperature).

of the strain amplitude, as shown in Fig. 16a. In the range between 0.01 and 50 % of strain amplitude it is possible to observe the low strain amplitude storage modulus plateau, a sharp reduction and a high strain amplitude storage modulus plateau for all tested materials. When this last plateau is not steadily reached, the value of E' at 100 % strain is considered indicative of the plateau level. Fig. 16 illustrates the storage modulus as function of strain amplitude as well as the storage modulus percentage reduction from the low deformation amplitude plateau to the high deformation amplitude plateau, commonly referred to as the Payne effect. It is possible to observe that the storage modulus, measured at low strain amplitude, decreases with increasing the slag content. This observation is supported by viscosity measurements and the tensile elastic modulus. When comparing NBR with different levels of slag content to standard NBRs of equal hardness, it is evident that standard NBR exhibits lower storage and loss moduli.

Notably, the storage modulus curve of NBR60 (0 % slag) exhibits the highest dynamic storage modulus across the entire range of strain amplitudes investigated, in comparison to NBR45 (100 % slag) and NBR50 (50 % slag). On the other hand, NBR50 (0 % slag) and NBR45 (0 % slag) show a less pronounced non-linear behavior. This non-linear effect or else Payne effect, is shown in Fig. 16b.

The Payne effect is believed to be associated with the filler-filler interaction and the rubber-filler interactions. Consequently, it is expected to increase with the CB content in standard NBRs due to the formation of a filler network and the larger surface area available for rubber-filler interactions (known as bound rubber) [61]. Consequently it is expected a Payne effect increase with increasing the CB content in standard NBRs due to the formation of a filler-filler network and the larger filler surface area [67]. It is interesting to note that NBR45 (100 % slag) shows a non-linear effect almost equivalent to that of NBR60 (0 %

slag), and higher than that of NBR50 (0 % slag) and NBR45 (0 % slag).

This behavior is assumed to be related to the interaction between slag and NBR, which appears to be effective despite the significant difference in grain size between CB and slag, resulting in a much smaller surface area for the slag.

4. Conclusion

CB is the most widely used as a reinforcing filler in rubber, but its production from the partial combustion of heavy hydrocarbons contributes to an enormous carbon footprint. Given the growing demand for rubber quality and the escalating cost of raw materials, there are several concerns regarding the traditional petroleum-based CB filler. Factors such as rising hydrocarbon prices and the non-degradability of petroleum-based CB pose significant environmental challenges. Consequently, the pursuit of sustainable alternatives to CB is crucial.

- For these reasons, sustainable alternatives to CB are being studied. The present study proposed the EAF slag, the main by-product of the steel industry, as a promising filler for NBR. The effect of slag as a substitute for CB both at equal filler volume fraction and equal hardness was investigated. The key findings can be summarized as follows: The slag mineralogical composition primarily consists of larnite, iron oxide, chromite in smaller quantities and minimal areas of brownmillerite.
- Incorporating EAF slag particles as filler in NBR matrix reduces the leaching of Cr, V, and Mo, as well as eluate pH and electrical conductivity. Consequently, the resulting compounds meet the criteria for reuse (Italian Ministerial Decree 5/4/06 [59]) and for disposal as inert material (Italian Ministerial Decree 30/8/05 [60]);
- The presence of slag as a CB replacement does not significantly affect the crosslinking kinetics, indicating comparable processability characteristics;
- The mechanical properties of slag filled compounds demonstrate their potential as alternatives to standard compounds in terms of both short and long term mechanical performance (viscoelastic and ageing behavior);
- Extensive investigations into the filler-matrix interaction, including crosslink density, bound rubber content of uncured compound and Payne effect, provide compelling evidence of interaction between slag and NBR.

In conclusion, the study established that EAF slag-filled NBRs can effectively be used as an alternative to standard compounds. Further research can focus on tailoring formulations to meet specific application requirements. Moreover, among the evident environmental benefits, also economic advantages may be drawn by the actors involved in this new application of EAF black slag: on one side the steel mills avoid the slag disposal cost and on the other side the rubber compounders incur a lower raw material cost.

CRediT authorship contribution statement

Anna Gobetti: Writing – review & editing, Writing – original draft, Visualization, Validation, Software, Resources, Project administration, Methodology, Investigation, Formal analysis, Data curation, Conceptualization. **Giovanna Cornacchia:** Visualization, Supervision, Methodology, Investigation, Funding acquisition, Formal analysis. **Silvia Agnelli:** Visualization, Validation. **Mattia Ramini:** Visualization. **Giorgio Ramorino:** Supervision, Project administration, Methodology, Investigation, Funding acquisition.

Declaration of competing interest

The authors declare that they have no known competing financial interests or personal relationships that could have appeared to influence the work reported in this paper.

Acknowledgements

The authors thank Ligom Spa for compounding the materials, Asonext Spa for providing the EAF slag and test equipment, and Italian Gasket for the cooperation.

References

[1] A.N. Gent, Engineering with rubber, third ed., Hanser Publishers, Munich, 2012. Doi:10.3139/9783446428713.fm.
[2] Y. Fan, G.D. Fowler, M. Zhao, The past, present and future of carbon black as a rubber reinforcing filler – a review, J. Clean. Prod. 247 (2020), https://doi.org/10.1016/j.jclepro.2019.119115.
[3] S.C. Peterson, S.R. Chandrasekaran, B.K. Sharma, Birchwood biochar as partial carbon black replacement in styrene-butadiene rubber composites, J. Elastomers Plast. 48 (2016) 305–316, https://doi.org/10.1177/0095244315576241.
[4] E. Athanassiades, Waste tyre pyrolysis: sustainable recovery and reuse of a valuable resource, PQDT - UK Irel. (2013).
[5] A. Gobetti, G. Ramorino, Application of short – term methods to estimate the environmental stress cracking resistance of recycled HDPE, J. Polym. Res. 27 (2020), https://doi.org/10.1007/s10965-020-02332-w.
[6] M. Battista, A. Gobetti, S. Agnelli, G. Ramorino, Post-consumer tires as a valuable resource: review of different types of material recovery, Environ. Technol. Rev. (2021), https://doi.org/10.1080/21622515.2020.1861109.
[7] A. Gobetti, G. Cornacchia, M. Gelfi, G. Ramorino, White steel slag from ladle furnace as calcium carbonate replacement for nitrile butadiene rubber: a possible industrial symbiosis, Results Eng. 18 (2023) 101229, https://doi.org/10.1016/j.rineng.2023.101229.
[8] N. Muttil, S. Jagadeesan, A. Chanda, M. Duke, S. Kumar Singh, Characterisation of activated carbon derived from carbon black produced by the pyrolysis of waste tyres, Adv. Mater. Process. Technol. (2023), https://doi.org/10.1080/2374068X.2023.2192327.
[9] Z.D. Hood, S.P. Adhikari, S.F. Evans, H. Wang, Y. Li, A.K. Naskar, M. Chi, A. Lachgar, M.P. Paranthaman, Tire-derived carbon for catalytic preparation of biofuels from feedstocks containing free fatty acids, Carbon Resour. Convers. 1 (2018) 165–173, https://doi.org/10.1016/j.crcon.2018.07.007.
[10] X. Ren, K. Cornish, Waste Conversion into Sustainable and Reinforcing Fillers for Rubber Composites, Elsevier Ltd. (2020), https://doi.org/10.1016/b978-0-12-803581-8.10547-8.
[11] G.R. Martín-Cortés, F.J. Esper, A.J. Santana de Araujo, W.T. Hennies, M.G. Silva Valenzuela, F.R. Valenzuela-Díaz, Replacement of carbon black on natural rubber composites and nanocomposites – part 1, in: Charact. Miner. Met. Mater. 2015, Springer International Publishing, 2016, pp. 145–152. https://doi.org/10.1007/978-3-319-48191-3_18.
[12] P. Yuvaraj, J.R. Rao, N.N. Fathima, N. Natchimuthu, R. Mohan, Complete replacement of carbon black filler in rubber sole with CaO embedded activated carbon derived from tannery solid waste, J. Clean. Prod. 170 (2018) 446–450, https://doi.org/10.1016/j.jclepro.2017.09.188.
[13] C. Li, F. Huang, J. Wang, X. Liang, S. Huang, J. Gu, Effects of partial replacement of carbon black with nanocrystalline cellulose on properties of natural rubber nanocomposites, J. Polym. Eng. 38 (2018) 137–146, https://doi.org/10.1515/polyeng-2016-0382.
[14] D. Bosch, J.O. Back, D. Gurtner, S. Giberti, A. Hofmann, A. Bockreis, Alternative feedstock for the production of activated carbon with ZnCl<inf>2</inf>: forestry residue biomass and waste wood, Carbon Resour. Convers. 5 (2022) 299–309, https://doi.org/10.1016/j.crcon.2022.09.001.
[15] M. Pisciotta, The volume expansion of artificial road aggregates derived from steelmaking slags, Eur. Transp. - Trasp. Eur. (2020).
[16] George C. Wang, The utilization of slag in civil infrastructure construction, 2014.
[17] A. Kavussi, M.J. Qazizadeh, Fatigue characterization of asphalt mixes containing electric arc furnace (EAF) steel slag subjected to long term aging, Constr. Build. Mater. 72 (2014) 158–166, https://doi.org/10.1016/j.conbuildmat.2014.08.052.
[18] J.A. Fuente-Alonso, V. Ortega-López, M. Skaf, Á. Aragón, J.T. San-José, Performance of fiber-reinforced EAF slag concrete for use in pavements, Constr. Build. Mater. 149 (2017) 629–638, https://doi.org/10.1016/j.conbuildmat.2017.05.174.
[19] C. Pellegrino, V. Gaddo, Mechanical and durability characteristics of concrete containing EAF slag as aggregate, Cem. Concr. Compos. 31 (2009) 663–671, https://doi.org/10.1016/j.cemconcomp.2009.05.006.
[20] Federacciai, Relazione Annuale 2021, 2021. https://federacciai.it/pubblicazioni-varie/.
[21] A. Gobetti, G. Cornacchia, G. Ramorino, A. Riboldi, L.E. Depero, EAF slag as alternative filler for epoxy screeds, an example of green reuse, Sustain. Mater. Technol. 29 (2021) e00324.
[22] A. Gobetti, G. Cornacchia, G. Ramorino, Innovative reuse of electric arc furnace slag as filler for different polymer matrixes, Minerals 11 (2021) 832, https://doi.org/10.3390/min11080832.
[23] A. Gobetti, G. Cornacchia, G. Ramorino, Reuse of electric arc furnace slag as filler for nitrile butadiene rubber, JOM 74 (2022) 1329–1339, https://doi.org/10.1007/s11837-021-05135-6.

[24] A. Gobetti, G. Cornacchia, M. La Monica, A. Zacco, L.E. Depero, G. Ramorino, Assessment of the influence of electric arc furnace slag as a non-conventional filler for Nitrile Butadiene Rubber, Results Eng. 17 (2023) 100987, https://doi.org/10.1016/j.rineng.2023.100987.
[25] A. Gobetti, G. Cornacchia, C. Petrogalli, R.C. Kerschbaumer, M. La Monica, G. Ramorino, Characterization of recycled end-of-life rubber tire filled with black slag, J. Reinf. Plast. Compos. (2023) 1–18, https://doi.org/10.1177/07316844231155398.
[26] G. Wypych, Handbook of Fillers: Fourth Edition, 2016. https://doi.org/10.1016/C2015-0-01953-0.
[27] J.B. Donnet, E. Custodero, Reinforcement of elastomers by particulate fillers, Sci. Technol. Rubber (2005), https://doi.org/10.1016/B978-012464786-2/50011-0.
[28] ASTM, ASTM D297 Chemical Analysis Test Procedures for Rubber Products, Am. Soc. Test. Mater. (2021).
[29] ASTM, D2240 Standard Test Method for Rubber Property—Durometer Hardness, Standard (2015).
[30] C. Navarro, M. Díaz, M.A. Villa-García, Physico-chemical characterization of steel slag. study of its behavior under simulated environmental conditions, Environ. Sci. Technol. 44 (2010), https://doi.org/10.1021/es100690b.
[31] UNI, EN 12457-2 Characterisation of waste – Leaching – Compliance test for leaching of granular waste materials and sludges – Part 2: One stage batch test at a liquid to solid ratio of 10 l/kg for materials with particle size below 4 mm (without or with size r), 2004.
[32] ASTM D5289, Rubber Property — Vulcanization Using Rotorless Cure, Astm (2015).
[33] K.L. Mok, A.H. Eng, Characterisation of crosslinks in vulcanised rubbers: From simple to advanced techniques, Malaysian J. Chem. 20 (2018) 118–127.
[34] F.A. Neugebauer, 9.1 Introduction, Nitrogen Oxyg, Centered Radicals (2006) 7–9, https://doi.org/10.1007/10858968_2.
[35] K. Sridharan, K. Elangovan, Investigation on the swelling characteristics of NR/BR rubber blends, J. Chem. Pharm. Res. 8 (2016) 553–557.
[36] M. Barikani, C. Hepburn, Determination of crosslink density by swelling in the castable polyurethane elastomer based on 1/4 – cyclohexane diisocyanate and para-phenylene diisocyanate, Iran. J. Polym. Sci. Technol. 1 (1992) 1–5.
[37] G.M. Bristow, W.F. Watson, Cohesive energy densities of polymers: Part 1. – Cohesive energy densities of rubbers by swelling measurements, Trans. Faraday Soc. (1958), https://doi.org/10.1039/TF9585401731.
[38] G.M. Bristow, W.F. Watson, Cohesive energy densities of polymers: Part 2. – Cohesive energy densities from viscosity measurements, Trans. Faraday Soc. (1958), https://doi.org/10.1039/TF9585401742.
[39] A.J. Marzocca, A.L. Rodriguez Garraza, P. Sorichetti, H.O. Mosca, Cure kinetics and swelling behaviour in polybutadiene rubber, Polym. Test. 29 (2010), https://doi.org/10.1016/j.polymertesting.2010.02.008.
[40] G. Kraus, Swelling of filler-reinforced, J. Appl. Polym. Sci. 7 (1963) 861–871.
[41] Y.S. Lee, S.H. Park, J.C. Lee, K. Ha, Influence of microstructure in nitrile polymer on curing characteristics and mechanical properties of carbon black-filled rubber composite for seal applications, J. Elastomers Plast. 48 (2016), https://doi.org/10.1177/0095244315613621.
[42] ISO 37, Rubber, vulcanized or thermoplastic—Determination of tensile stress-strain properties, 2017.
[43] ISO 7743:2011, Rubber, vulcanized or thermoplastic—Determination of compression stress-strain properties, Standards 3 (2011).
[44] M. Tossavainen, F. Engstrom, Q. Yang, N. Menad, M. Lidstrom Larsson, B. Bjorkman, Characteristics of steel slag under different cooling conditions, Waste Manag. 27 (2007) 1335–1344, https://doi.org/10.1016/j.wasman.2006.08.002.
[45] F. Engström, D. Adolfsson, Q. Yang, C. Samuelsson, B. Björkman, Crystallization behaviour of some steelmaking slags, Steel Res. Int. 81 (2010) 362, https://doi.org/10.1002/srin.200900154.
[46] D. Mombelli, A. Gruttadauria, S. Barella, C. Mapelli, The influence of slag tapping method on the efficiency of stabilization treatment of electric arc furnace carbon steel slag (EAF-C), Minerals 9 (2019) 706, https://doi.org/10.3390/min9110706.
[47] D. Mombelli, C. Mapelli, S. Barella, C. Di Cecca, G. Le Saout, E. Garcia-Diaz, The effect of chemical composition on the leaching behaviour of electric arc furnace (EAF) carbon steel slag during a standard leaching test, J. Environ. Chem. Eng. 4 (2016) 1050–1060, https://doi.org/10.1016/j.jece.2015.09.018.
[48] D. Mombelli, C. Mapelli, C. Di Cecca, S. Barella, A. Gruttadauria, Electric arc furnace slag: study on leaching mechanisms and stabilization treatments | Scorie da forno elettrico ad arco: Studio sui meccanismi di rilascio e trattamenti di stabilizzazione, Metall. Ital. 108 (2016) 5–17.
[49] H.W. Kilau, I.D. Shah, Preventing chromium leaching from waste slag exposed to simulated acid precipitation: a laboratory study, Rep. Investig. – United States, Bur. Mines (1984).
[50] H. Cabrera-Real, A. Romero-Serrano, B. Zeifert, A. Hernandez-Ramirez, M. Hallen-Lopez, A. Cruz-Ramirez, Effect of MgO and CaO/SiO on the immobilization of chromium in synthetic slags, J. Mater. Cycles Waste Manag. 14 (2012) 317–324, https://doi.org/10.1007/s10163-012-0072-y.
[51] V. Arredondo-Torres, A. Romero-Serrano, B. Zeifert, J. Cruz-Rivera, P. Flores-Sánchez, A. Cruz-Ramírez, Stabilization of MgCr2O4 spinel in slags of the SiO2-CaO-MgO-Cr2O3 system, Rev. Metal. 42 (2006) 417–424.
[52] D. Mombelli, S. Barella, A. Gruttadauria, C. Mapelli, G. Le Saout, E. Garcia-Diaz, Effects of basicity and mesh on Cr leaching of EAF carbon steel slag, Appl. Sci. 9 (2018), https://doi.org/10.3390/app9010121.
[53] D. Mombelli, C. Mapelli, S. Barella, C. Di Cecca, G. Le Saout, E. Garcia-Diaz, The effect of microstructure on the leaching behaviour of electric arc furnace (EAF) carbon steel slag, Process Saf. Environ. Prot. 102 (2016) 810–821, https://doi.org/10.1016/j.psep.2016.05.027.
[54] R.R. Gelfi M., Cornacchia G., Investigations on leaching behavior of EAF steel slags, in: Electr. Arc Furn. Slag, 2010.
[55] A. Adib, C. Domínguez, J. Rodríguez, C. Martín, R.A. García, The effect of microstructure on the slow crack growth resistance in polyethylene resins, Polym. Eng. Sci. 55 (2015) 1018–1023, https://doi.org/10.1002/pen.23970.
[56] I. Strandkvist, K. Pålsson, A. Andersson, J. Olofsson, A. Lennartsson, C. Samuelsson, F. Engström, Minimizing chromium leaching from low-alloy electric arc furnace (EAF) slag by adjusting the basicity and cooling rate to control brownmillerite formation, Appl. Sci. 10 (2020), https://doi.org/10.3390/app10010035.
[57] A. Riboldi, G. Cornacchia, M. Gelfi, L. Borgese, A. Zacco, E. Bontempi, M. V. Boniardi, A. Casaroli, L.E. Depero, Grain size effect in elution test of electric arc furnace slag, Appl. Sci. 10 (2020), https://doi.org/10.3390/app10020477.
[58] G. Geißler, S. Schüler, T. Raiger, D. Mudersbach, H.P. Markus, D. Algermissen, Factors of influence during and after the electric steel making process: Characterization and optimization of electric arc furnace slag. Proc. 8th Eur. Slag Conf. EUROSLAG, Linz (Austria), 2015.
[59] n. 115 Ministero della tutela dell'ambiente e del territorio Gazzetta Ufficiale 19 maggio 2006, Individuazione dei rifiuti non pericolosi sottoposti alle procedure semplificate di recupero, ai sensi degli articoli 31 e 33 del decreto legislativo 5 febbraio 1997, n. 22, Italia, n.d.
[60] n. 201 Ministero della tutela dell'ambiente e del territorio Gazzetta Ufficiale del 30 agosto 2005, Definizione dei criteri di ammissibilità dei rifiuti in discarica, Italia, n. d.
[61] S. Zhang, R. Zhong, R. Hong, D. Hui, On factors affecting surface free energy of carbon black for reinforcing rubber, Nanotechnol. Rev. 9 (2020), https://doi.org/10.1515/ntrev-2020-0015.
[62] C. Gauthier, E. Reynaud, R. Vassoille, L. Ladouce-Stelandre, Analysis of the non-linear viscoelastic behaviour of silica filled styrene butadiene rubber, Polymer (guildf) 45 (2004) 2761–2771, https://doi.org/10.1016/j.polymer.2003.12.081.
[63] S. Thomas, S.C. George, S. Thomas, Rigid amorphous phase: Mechanical and transport properties of nitrile rubber/clay nanocomposites, Prog. Rubber Plast. Recycl. Technol. 33 (2017) 103–126, https://doi.org/10.1177/147776061703300204.
[64] P.J.P.J. Flory, J. Rehner, J. Rehner Jr., Statistical mechanics of cross-linked polymer networks II. Swelling, J. Chem. Phys. 11 (1943) 521–526, https://doi.org/10.1063/1.1723792.
[65] S.Y. Lee, S. Bin Eom, J.S. Won, J.W. Bae, S.H. Park, S.G. Lee, Evaluation of aging behavior of nitrile butadiene rubbers via oxygen-consumption experiments, Fibers Polym. 22 (2021), https://doi.org/10.1007/s12221-021-0345-y.
[66] J. Diani, B. Fayolle, P. Gilormini, A review on the Mullins effect, Eur. Polym. J. 45 (2009), https://doi.org/10.1016/j.eurpolymj.2008.11.017.
[67] S.S. Sternstein, A.-J. Zhu, Reinforcement mechanism of nanofilled polymer melts as elucidated by nonlinear viscoelastic behavior, Macromolecules 35 (2002) 7262–7273, https://doi.org/10.1021/ma020482u.